PHYSICAL REVIEW B **75**, 054513 (2007)

Superconductivity in gallium-substituted Ba_8Si_{46} clathrates

Yang Li,[1,2,3,*] Ruihong Zhang,[1] Yang Liu,[1] Ning Chen,[1] Z. P. Luo,[4] Xingqiao Ma,[1] Guohui Cao,[1] Z. S. Feng,[5] Chia-Ren Hu,[3] and Joseph H. Ross, Jr.[3,*]

[1]*Department of Physics, University of Science and Technology Beijing, Beijing 100083, China*

[2]*Department of Engineering Science and Materials, University of Puerto Rico at Mayaguez, Mayaguez, Puerto Rico 00681-9044, USA*

[3]*Department of Physics, Texas A&M University, College Station, Texas 77843-4242, USA*

[4]*Microscopy and Imaging Center, Texas A&M University, College Station, Texas 77843-2257, USA*

[5]*Department of Mathematics, University of Texas–Pan American, Edinburg, Texas 78541, USA*

(Received 25 October 2006; published 16 February 2007)

We report a joint experimental and theoretical investigation of superconductivity in Ga-substituted type-I silicon clathrates. We prepared samples of the general formula $Ba_8Si_{46-x}Ga_x$, with different values of x. We show that $Ba_8Si_{40}Ga_6$ is a bulk superconductor, with an onset at $T_C \approx 3.3$ K. For $x=10$ and higher, no superconductivity was observed down to $T=1.8$ K. This represents a strong suppression of superconductivity with increasing Ga content, compared to Ba_8Si_{46} with $T_C \approx 8$ K. Suppression of superconductivity can be attributed primarily to a decrease in the density of states at the Fermi level, caused by a reduced integrity of the sp^3-hybridized networks as well as the lowering of carrier concentration. These results are corroborated by first-principles calculations, which show that Ga substitution results in a large decrease of the electronic density of states at the Fermi level, which explains the decreased superconducting critical temperature within the BCS framework. To further characterize the superconducting state, we carried out magnetic measurements showing $Ba_8Si_{40}Ga_6$ to be a type-II superconductor. The critical magnetic fields were measured to be $H_{C1} \approx 35$ Oe and $H_{C2} \approx 8.5$ kOe. We deduce the London penetration depth $\lambda \approx 3700$ Å and the coherence length $\xi_c \approx 200$ Å. Our estimate of the electron-phonon coupling reveals that $Ba_8Si_{40}Ga_6$ is a moderate phonon-mediated BCS superconductor.

DOI: 10.1103/PhysRevB.75.054513 PACS number(s): 74.70.Wz, 73.61.Wp, 61.48.+c, 71.20.Tx

I. INTRODUCTION

Group-IV clathrate materials are extended Si, Ge, and Sn cagelike solids with sp^3-hybridized networks, which have received increasing attention over the past few years. These materials have a semiconducting framework into which metal atoms can be substituted, providing a number of possibilities for electronic materials.[1,2] Furthermore, within the sp^3-hybridized networks, K, Na, Rb, Cs, Sr, Ba, I, and Eu atoms can be encapsulated in the cages.[3,4] Clathrates exhibit metallic, semiconducting, or insulating behavior depending upon the occupation fraction, and on the substitution of atoms in the cage framework to replace the group-IV atoms. The study of clathrates opens a field of new materials with the metals arranged in such a nanoscale array, and with a wide variety of properties ranging from insulators to metals.[5] New thermoelectric applications have driven a great deal of this increased current interest.[6,7] The materials can be adjusted from semiconducting to metallic, while at the same time the cage structures can be filled with atoms that strongly scatter phonons. These factors greatly influence the thermoelectric efficiency. Recently, NMR and Mössbauer measurements have directly demonstrated atomic hopping within the cages of $Sr_8Ge_{30}Ga_{16}$ (Ref. 8) and $Eu_8Ge_{30}Ga_{16}$,[9] respectively. The variety of electronic behavior attained by chemical substitution and doping suggests that significant new features may be produced in this system. In a search for better phonon scattering efficiency, Ge clathrates filled with the rare earth Eu have been synthesized, indicating that clathrates of this type containing local magnetic moments are possible.[10] Further studies have identified ferromagnetic behavior in magnetically substituted $Ba_8Mn_4Ge_{42}$ (type-I clathrate) (Ref. 11) and $Ba_6Fe_3Ge_{22}$ (chiral-type clathrate).[12] The potential of such magnetic clathrates is quite significant, since the clathrate structure can be adjusted for the tailoring of magnetic properties by substitution and alloying. Therefore clathrates also have potential application in magnetic sensors and new magnetic semiconductors.[12–14]

Inspired by the discovery of superconductivity in alkali-metal-doped C_{60} fullerenes, efforts have been made to explore the superconductivity of group-IV clathrates with particular attention to the sp^3-hybridized networks. In contrast to carbon, silicon and germanium do not form sp^2-like networks. Therefore, superconductivity of Si clathrate superconductors with the sp^3 network should be unique. In an initial study, Caplin and co-workers investigated the conductivity and magnetic susceptibility of silicon clathrates containing Na atoms as guests,[5] but found no superconductivity in these materials. However, Ba-encapsulated silicon clathrates were found to exhibit superconductivity, with $T_C \sim 8$ K for the best samples with pure Ba encapsulation.[15,16] This kind of superconductor is unusual in that the structure is dominated by strong covalent bonds between silicon atoms, rather than the metallic bonding that is more typical of traditional superconductors. Isotope effect measurements revealed that superconductivity in Ba_8Si_{46} is of the classic BCS kind, arising from the electron-phonon interaction.[17] Study of the band structure for Ba_8Si_{46} showed a strong hybridization between the Si_{46} band and Ba orbitals, resulting in a very high density of states at the Fermi level, $N(E_F) \sim 40$ states/eV per unit cell.[18–20] Both the strong hybridization of Ba with the conduction band and the high $N(E_F)$ are believed to play a key

role in the superconductivity of these compounds, and further studies of Si and Ge clathrates indicate the superconductivity to be an intrinsic property of the sp^3 network.[20,21]

We are interested in the effect of Ga on the superconductivity of Ba_8Si_{46}, as well as the change of electronic structure in the clathrates. The $Ba_8(Si,Ga)_{46}$ system exhibits a wide variety of physical properties; with the Ga content increasing from $x=0$, the clathrate behavior changes from superconducting Ba_8Si_{46} ($T_C \sim 8$ K) (Ref. 17) to the heavily doped semiconductor $Ba_8Si_{30}Ga_{16}$.[22] Investigation of Ga doping can also increase our understanding of the electronic structure and superconducting mechanism in clathrate materials.

In this paper, we report a joint experimental and theoretical study of Ga substitution in $Ba_8Si_{46-x}Ga_x$ clathrates. We show that $Ba_8Si_{40}Ga_6$ is a bulk type-II superconductor; however, with increasing Ga content, the superconducting T_C decreases rapidly, and with $x=10$ or more, there is no evidence of superconductivity for temperatures as low as 1.8 K. We also used first-principles calculations to build a detailed picture of the atomic and electronic structure of Ga-substituted clathrates. By comparing the electronic structures of different Ga-substituted silicon clathrates, our theoretical results show that Ga doping gives rise to a lower density of states at the Fermi level $[N(E_F)]$, which was explained as one of the reasons for the destructive effect of Ga doping on superconductivity in Si clathrates. For dilute levels, we show that the changes induced by substitution of Ga for Si are approximately rigid band in character, so that it is possible to change the electron concentration by framework substitution while leaving the superconducting character of the sp^3 network intact.

II. EXPERIMENTAL RESULTS

Our synthesis of $Ba_8Si_{46-x}Ga_x$ is based on the multistep melting of Ba, Ga, and Si under argon atmosphere and subsequent solid-state reaction.[12] The samples were characterized and analyzed by x-ray diffraction and transmission electron microscopy. The obtained samples were then analyzed for magnetic properties by a superconducting quantum interference device (SQUID) magnetometer.

Analysis by powder x-ray diffraction showed characteristic type-I clathrate reflections. Structural refinement of the powder x-ray diffraction data was carried out using the GSAS software package.[23,24] As a result of the refinement, we find that for dilute doping, Ga preferentially occupies the 6*c* framework sites; however, for heavy substitution, Ga tends to a random distribution of the other sites. This is similar to the site occupancy identified for $Ba_8Ga_{16}Ge_{30}$,[25] and for $Ba_8Ga_{16}Si_{30}$,[26] although the latter work also identified a somewhat weaker preference for Ga on the 24*k* site as well. As shown in the left inset of Fig. 1, the refined lattice parameters of $Ba_8Si_{46-x}Ga_x$ ($x=6$, 10, and 16) are 10.4261, 10.4896, and 10.5096 Å, respectively, which exhibit an increasing trend with x due to the larger atomic size of Ga than that of Si. This is consistent with the results previously reported.[27]

For dilute Ga doping, the sample of $Ba_8Si_{40}Ga_6$ exhibited no additional phases when analyzed by x-ray diffraction at room temperature, as shown in Fig. 1. $Ba_8Si_{40}Ga_6$ crystallizes into the type-I clathrate structure [cubic space group $Pm\bar{3}n$ (No. 223)] with dimension $a=10.4261$ Å. The experimental pattern is in agreement with the simulated one for the entire 2θ region. R values for the fit are $R_{wp}=0.12$, $R_p=0.09$. The measured structural parameters were selected as the input data for the model simulations. The samples with $x=10$ and 16 similarly exhibited single-phase x-ray patterns.

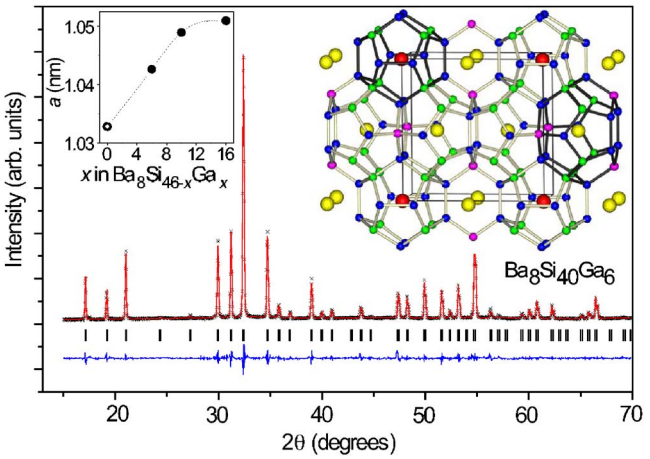

FIG. 1. (Color online) X-ray refinement for $Ba_8Si_{40}Ga_6$. Upper curve: data and fit, with difference plot below. Ticks show peaks indexed according to the type-I clathrate structure. Right inset: the type-I clathrate structure, built from a regular arrangement of a combination of Si_{20} (I_h) and Si_{24} (D_{6d}) cages. Left inset: lattice parameters of $Ba_8Si_{46-x}Ga_x$ ($x=6$, 10, and 16), showing an increasing trend with x. The lattice parameter for Ga-free Ba_8Si_{46} clathrate was taken from Ref. 16.

Transmission electron microscopy (TEM) measurements were carried out in a JEOL 2010 electron microscope at a voltage of 200 kV, with an Oxford Instruments INCA energy-dispersive spectroscopy (EDS) system for chemical compositional analysis. In order to obtain accurate quantification, the k factor (ratio to Si, $k_{Si}=1$) of Ga and Ba were corrected during the quantification process using the INCA program.[28] TEM observations confirmed that the majority phase has the clathrate structure, with space group $Pm\bar{3}n$. Figure 2 displays three electron diffraction patterns taken from the clathrate structure along the [111], [112], and [113] zone axes. The reflection intensities are consistent with dynamic electron diffraction simulations according to the clathrate structure.[28] Chemical compositional analyses of three samples with nominal compositions of $Ba_8Si_{40}Ga_6$, $Ba_8Si_{36}Ga_{10}$, and $Ba_8Si_{30}Ga_{16}$ were performed on particles selected by the electron diffraction to confirm the clathrate structure. A comparison of EDS results is given in Table I. It is seen that the quantification results are very consistent with the sample nominal compositions.

Figure 3 shows the temperature dependence of the ac susceptibility of the $Ba_8Si_{40}Ga_6$ sample, measured in zero static field at a frequency of 125 Hz. The susceptibility shows hardly any temperature dependence for $300>T>4$ K. At about 3.3 K, the sample starts to show superconducting characteristics; the in-phase susceptibility (χ') suddenly drops and the out-of-phase susceptibility (χ'') peaks. These large

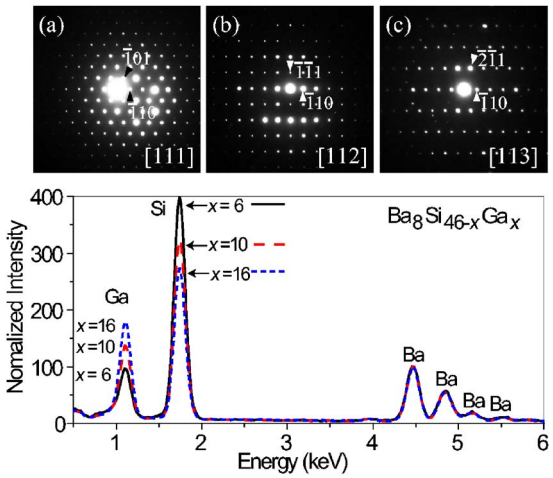

FIG. 2. (Color online) Upper figure: Electron diffraction patterns from the clathrate structure along the [111] (a), [112] (b), and [113] (c) axis. Lower figure: Comparison of EDS spectra from samples $Ba_8Si_{40}Ga_6$ (solid curve), $Ba_8Si_{36}Ga_{10}$ (long-dashed curve), and $Ba_8Si_{30}Ga_{16}$ (short-dashed curve). The intensities are normalized to the lowest-energy Ba peak to reveal the variation of the Si-Ga ratio.

changes in the susceptibility are accompanied by a distinct drop in electrical resistivity of the $Ba_8Si_{40}Ga_6$ sample; four-probe transport measurements using a Lake Shore Physical Property Measurement System confirm that $Ba_8Si_{40}Ga_6$ enters into a superconducting state at 3.3 K. The resistance sharply drops from its high temperature value of $R=7$ mΩ to zero resistance, as shown in Fig. 4. A change in the temperature slope from metallic to semiconducting type at about 50 K is also observed above the superconducting transition temperature. A measurement at a high field of 70 kOe also demonstrates the metal-semiconductor slope change, as shown in the inset to Fig. 4, however with a smaller overall resistance in high field. No sign of superconductivity was observed in high field; 70 kOe exceeds the critical field as discussed below. Within the standard BCS approach to superconductivity, as has been applied for other superconducting Si clathrates,[17] we deduce the value of the superconducting gap at 0 K from the critical temperature ($T_C=3.3$ K) using the well-known relation[29] $2\Delta_{T\to 0\ \mathrm{K}}=3.52k_BT_C$. In this way we find that the superconducting gap is about 0.5 meV for $Ba_8Si_{40}Ga_6$.

The inset of Fig. 3 presents the dc susceptibility of $Ba_8Si_{40}Ga_6$ as a function of temperature, under conditions of zero-field cooling (ZFC) and field cooling (FC) at 3 Oe. The ZFC magnetization data were taken on heating after sample cooling in zero applied field, and the FC magnetization was

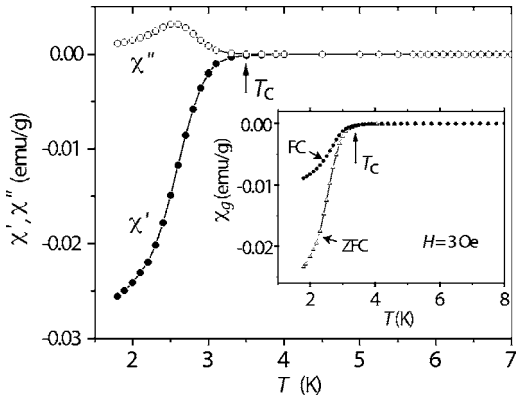

FIG. 3. ac and dc magnetic susceptibility of $Ba_8Si_{40}Ga_6$ vs temperature. Main plot: temperature dependence of the in-phase (χ') and out-of-phase (χ'') ac susceptibility, measured in zero dc field. Inset: dc susceptibility for conditions of zero-field cooling (ZFC) and field cooling (FC) in the measurement field of 3 Oe. The onset superconducting transition is observed at 3.3 K as shown.

measured as a function of decreasing temperature in the applied field. The enhancement of the diamagnetism below $T_C(H)$ originates from the screening supercurrents (ZFC regime) and the Meissner effect of magnetic flux expulsion (FC regime). The inset figure demonstrates that there is a difference between χ_g in ZFC and FC conditions. As can be seen from the plot, for both ZFC and FC, χ_g exhibits a superconducting drop for $T<T_C$. The T_C (=3.3 K) found for $Ba_8Si_{40}Ga_6$ is lower than that of pure Ba_8Si_{46} ($T_C=4-8$ K depending on sample preparation).[15,16] However, for this case, where the Ga substitution for Si is 13 at. %, T_C is not very strongly suppressed, a result that is quite different from Cu doping in Ba_8Si_{46}.[20] For example, in $Ba_8Si_{42}Cu_4$ the onset T_C is reduced to 2.9 K while for $Ba_8Si_{40}Cu_6$ no superconductivity was observed down to 1.8 K. It is clear that the similarity of Ga and Si in electronic structure helps to maintain the superconducting sp^3 network. Our theoretical simulations discussed below also demonstrate this result. Also, as shown in Fig. 3, the existence of the hysteresis between the two magnetization curves for the zero-field-cooling and the field-cooling modes indicates that the compound is a type-II superconductor.

As shown in Fig. 3, the superconducting onset temperature is 3.3 K, while the bulk transition occurs at around $T=2.6$ K. The superconducting volume fraction was estimated to be 96% of the theoretical Meissner value according to the ZFC susceptibility, and 36% of theoretical for the FC curve. For these estimates, the theoretical density of 3.9 g/cm^3 was used, as estimated from the x-ray diffraction (XRD) data for $Ba_8Si_{40}Ga_6$. Furthermore, the sample was roughly a half

TABLE I. EDS quantitative analysis results.

Nominal composition	Ba (at. %)	Si (at. %)	Ga (at. %)	Measured chemical formula
$Ba_8Si_{40}Ga_6$	14.9±1.5	74.7±2.1	10.4±1.0	$Ba_{8.0\pm0.8}Si_{40.3\pm1.1}Ga_{5.6\pm0.5}$
$Ba_8Si_{36}Ga_{10}$	14.9±1.1	66.1±2.5	19.0±1.4	$Ba_{8.0\pm0.6}Si_{35.7\pm1.4}Ga_{10.3\pm0.8}$
$Ba_8Si_{30}Ga_{16}$	15.9±1.2	57.7±5.0	26.4±4.0	$Ba_{8.6\pm0.6}Si_{31.2\pm2.7}Ga_{14.3\pm2.2}$

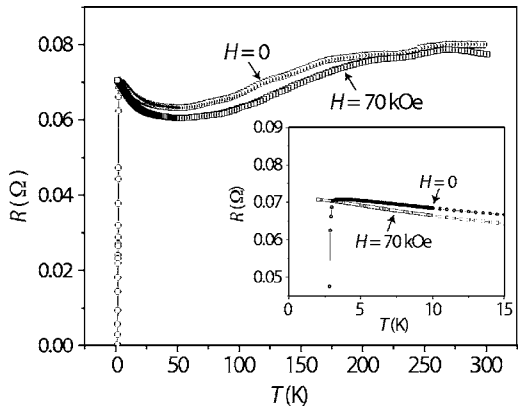

FIG. 4. Resistance of $Ba_8Si_{40}Ga_6$ versus temperature at $H=0$ and 70 kOe. Inset: magnified view of the low-temperature region, for clarity. The onset superconducting transition is observed at 3.3 K.

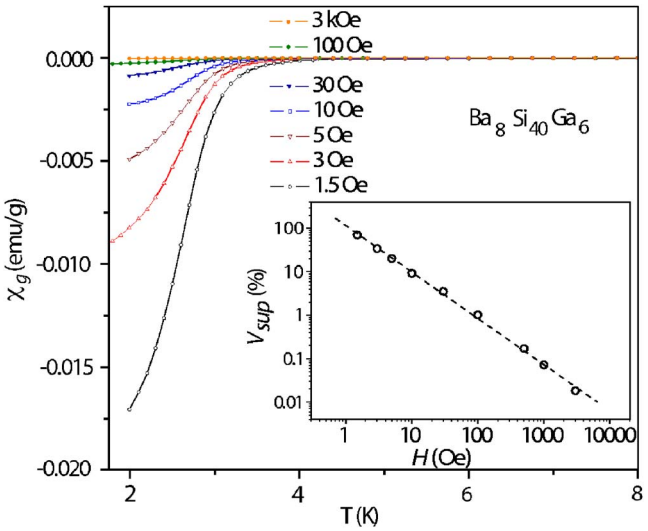

FIG. 5. (Color online) FC susceptibility under different fields for $Ba_8Si_{40}Ga_6$. Inset: Meissner superconducting volume (V_{sup}) decreasing with external field according to log-linear behavior, with the fitted curve $\log_{10} V_{sup}=a+b \log_{10} H$.

disk, with measurements made parallel to the long axis, so we estimated the demagnetization factor (N) for this direction to be about 2 in cgs units. In this case the value $-1/(4\pi-N)$ corresponds to the bulk ideal Meissner effect, and we find that χ_{FC} is 36% of this value, representing a lower-bound estimate for the true superconducting volume fraction. The corresponding value obtained from ZFC measurements, 96% of theoretical, is an approximate upper bound for $T=1.8$ K. These results indicate that $Ba_8Si_{40}Ga_6$ is a bulk superconductor. This is compatible with the finding of nearly pure-phase clathrate based on electron microscopy and XRD phase analysis. By contrast, we found no evidence for a transition to a superconducting state in $Ba_8Si_{36}Ga_{10}$ and $Ba_8Si_{30}Ga_{16}$ from measurements down to 1.8 K, so clearly the substitution of Ga for Si by more than 20% heavily suppresses superconductivity in this system.

Temperature-dependent FC magnetization values under different magnetic fields are shown in Fig. 5. Flux expulsion (Meissner effect) decreases with increasing external field; the magnetic field easily suppresses the magnitude of superconducting response. We observed that with increasing applied field there occurs only a small suppression in T_C but a strong reduction in superconducting volume, as shown in the inset of Fig. 5. The Meissner superconducting volume V_{sup} decreases with increasing field in a log-linear behavior, $\log_{10} V_{sup}=a+b \log_{10} H$, with $a=0.065$ and $b=-1.068$.

To determine the superconducting critical fields H_{C1} and notably H_{C2}, the field dependence of the magnetization was measured. Evidence for a type-II superconducting state can be seen in Fig. 6(a) where we have plotted the M-H loop for $T=1.8$ K. As shown in Fig. 6(b), at small fields, the shielding is 100% and M versus H is approximately linear. At large fields, flux penetrates in the form of vortices and $|M|$ decreases. At 1.8 K, we estimate H_{C1} as the field where flux first penetrates into the sample, and the magnetization departs from linearity. This occurs at an applied field of approximately 21 Oe, as shown by an arrow in Fig. 6(b). The initial magnetization curve at $T=2$ K is also shown in Fig. 6(b). We estimate an approximate value of $H_{C1}\sim 35$ Oe by extrapolation to $T=0$ K, including the demagnetization effect.

We have determined the upper critical field H_{C2} from the field variation of the dc magnetization at high field. H_{C2} was estimated by the magnetic field at which the M-H reverse legs merge at high field, as shown in Fig. 6(c). The criterion of $|\Delta M|<10^{-4}$ emu/g was used for the determination of H_{C2}, which was determined to be 8.5 kOe.

From the estimates of H_{C1} and H_{C2}, we can determine the penetration depth λ and the coherence length ξ using the Ginzburg-Landau equations[30] $\mu_0 H_{C2}=\Phi_0/2\pi\xi^2$ and $\mu_0 H_{C1}=(\Phi_0/4\pi\lambda^2)[\ln(\lambda/\xi)+C_1]$ where $\kappa=\lambda/\xi$ is the Ginzburg-Landau parameter, $\Phi_0=\pi\hbar c/e$ is the flux quantum, and $C_1=0.497$.[31] From $H_{C1}\approx 35$ Oe and $H_{C2}\approx 8.5$ kOe, we obtain $\lambda\approx 4000$ Å and $\xi\approx 200$ Å. Hence, we find $\kappa\approx 20$. These values can be compared to those obtained for Ba_8Si_{46} ($\lambda\approx 4000$ Å, $\xi\approx 72$ Å, and $\kappa\approx 56$).[32] We found that both materials have the same order of magnitude for λ; however, ξ for the Ga-substituted material is three times larger than that of Ba_8Si_{46}. We can also remark that in the type-IX chiral-structure clathrate $Ba_{24}Ge_{100}$, $\lambda\approx 6500$ Å and $\xi\approx 310$ Å (Ref. 33) are similar to the values for $Ba_8Si_{40}Ga_6$ reported here.

III. THEORETICAL RESULTS

In order to explain the effect of Ga doping on superconductivity, first-principles calculations for the periodic boundary systems were carried out using the CASTEP code with the generalized gradient approximation (GGA). CASTEP are first-principles *ab initio* calculation packages, using plane-wave basis sets and suited for periodic systems. The total energy is minimized with respect to occupied orbitals using a conjugate-gradient method. Either the local density approximation (LDA) or GGA may be used to calculate the exchange and correlation energy of the electrons. Pseudopotentials are used to model the interaction of the valence electrons with the core of each atom. The total energy

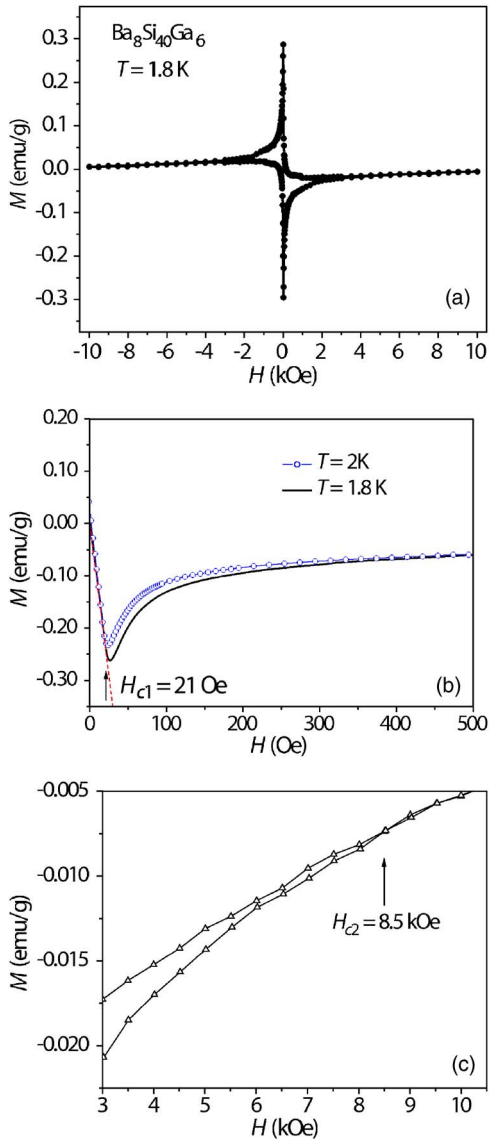

FIG. 6. (Color online) (a) M-H hysteresis of $Ba_8Si_{40}Ga_6$ at 1.8 K. (b) Initial magnetization curve at $T=1.8$ and 2 K, respectively. The lower critical field H_{C1} is determined from the departure from linearity at low field, which occurs at an applied field of approximately 21 Oe corresponding to 1.8 K. (c) M-H reverse legs merge at high field. The upper critical field H_{C2} was estimated to be 8.5 kOe at 1.8 K.

pseudopotential method we used was developed by Payne *et al.*[34] This method is based on density functional theory in describing the electron-electron interaction and on a pseudopotential description of the electron-core interaction, and has been publicized as CASTEP. It gives the total electronic energy of a large system, as well as its band structure. Transferability and robustness of the assumed pseudopotentials of each element seem to be confirmed by the success in reproducing the physical properties such as lattice parameters of many compounds. Therefore, it can be expected to give the relative stability of different crystal structures. We used the CASTEP code in order to solve the pseudopotential Schrödinger equation self-consistently. Besides the Ga-doped Si clathrates mentioned above, Ga-doped germanium clathrates were also calculated as a reference in order to check the suitability of the model parameters.

Wave functions were expanded in plane-wave basis sets with a kinetic energy cutoff of 300 eV for all systems studied. We adopted the ultrasoft pseudopotential. Calculated final structural data and inequivalent atomic positions of each model in the calculation are listed in Table II. The input structural parameters were obtained from experimental parameters by the geometry optimization function. As discussed above, x-ray diffraction refinement has shown that for dilute doping Ga is preferentially placed at the 6c site in clathrates. In order to simplify the Ga-substitution model and to give prominence to Ga substitution on 6*c* sites which bridge the Si_{20} and Si_{24} cages, we assumed Ga to be located on all the 6*c* sites for $Ba_8Si_{40}Ga_6$, and to occupy 16*i* and 24*k* sites with random distribution for $Ba_8Si_{36}Ga_{10}$ and $Ba_8Si_{30}Ga_{16}$. Spin polarization was not considered.

The band structure and density of states for $Ba_8Si_{40}Ga_6$ and $Ba_8Si_{30}Ga_{16}$ are shown in Fig. 7. For $Ba_8Si_{40}Ga_6$ $N(E)$ exhibits metallic character; the fundamental gap, with width about 0.7 eV, is located well below E_F. The Fermi level for $Ba_8Si_{40}Ga_6$ is positioned just below the maximum of a large $N(E)$ peak. Our calculations show a nearly identical peak for Ba_8Si_{46}, with peak value of about 38 states/eV; however, E_F is larger in Ba_8Si_{46} due to the larger number of valence electrons. This sharp peak is very close to what has previously been calculated for Ba_8Si_{46}, with reported peak ~40 states/eV.[20,35] The small reduction in $N(E_F)$ due to the lower valence count is consistent with the observed change in T_c, in the BCS model for superconductivity. Thus for dilute substitution of Ga, we find a nearly rigid-band displacement of the Fermi level, leaving the sp^3-connected electronic structure of the framework relatively unchanged and still conducive to superconductivity. However, for more heavily substituted $Ba_8Si_{30}Ga_{16}$, larger changes in electronic structure are observed. In the latter material the Fermi level is located just below the fundamental gap, according to the expected semiconducting behavior, since the temperature dependence of electrical resistivity of $Ba_8Si_{30}Ga_{16}$ is typical for heavily doped semiconductors. The results are similar to those obtained previously for this composition.[36]

A comparison of the band structures and $N(E)$ of $Ba_8Si_{40}Ga_6$ and $Ba_8Si_{30}Ga_{16}$ shows that there are significant changes brought about by the additional substitution of Ga. The valence and conduction bands are broadened, and the fundamental gap correspondingly narrowed. The band broadening may be understood as due to enhanced hybridization of the framework orbitals due to the more extended size of the Ga ion. This is similar to the effect of pressure on Ba_8Si_{46}, which also reduces T_c as the lattice constant is reduced.[37] $Ba_8Si_{30}Ga_{16}$ is a Zintl compound, as there are nominally 184 valence electrons in $Ba_8Si_{30}Ga_{16}$, contributing an average of four electrons for every framework atom, enough for a completely filled four-bonded network. Indeed, the simulation shows a lower total energy for $Ba_8Si_{40}Ga_6$ than Ba_8Si_{46} implying that the Ga-substituted phase is more stable. An additional stabilization, besides the Zintl mechanism, may come from the increased polarity of the Ga-Si bonds, as experimentally we find that the Ga-substituted materials can be formed more easily as single-phase materials, as compared to

TABLE II. Calculated equilibrium structures and inequivalent atomic positions for clathrate phases $Ba_8Si_{40}Ga_6$, $Ba_8Si_{36}Ga_{10}$, and $Ba_8Si_{30}Ga_{16}$. The notation for atomic positions follows that of the International Tables for Crystallography.

	$Ba_8Si_{40}Ga_6$	$Ba_8Si_{36}Ga_{10}$	$Ba_8Si_{30}Ga_{16}$
Symmetry	$Pm\bar{3}n$ (No. 223)	$P1$ (No. 1)	$P1$ (No. 1)
Lattice constant a (Å)	10.4261	10.4896	10.5096
6*c* (Ga)	x=0.25, y=0, z=0.5	x=0.25, y=0, z=0.5	x=0.25, y=0, z=0.5
16*i* (Si, Ga)	x,y,z=0.1823	x,y,z=0.1851	x,y,z=0.1877
24*k* (Si, Ga)	x=0.3034, y=0.1235, z=0	x=0, y=0.3075, z=0.1194	x=0, y=0.3103, z=0.1166
2*a* (Ba)	x,y,z=0	x,y,z=0	x,y,z=0
6*d* (Ba)	x=0.25, y=0.5, z=0	x=0.25, y=0.5, z=0	x=0.25, y=0.5, z=0

Ba_8Si_{46} which generally requires high-pressure techniques, and this is true even with relatively dilute Ga substitution. The fact that E_F falls just below the fundamental gap presumably reflects a slightly reduced negative charge on the Ba ions, as compared to the value (−2) expected from the nominal valence.

The presence of regions with localized polar bonds of tetravalent Si and trivalent Ga atoms is further supported by analysis of the calculated electron charge density. The difference between $Ba_8Si_{40}Ga_6$ and $Ba_8Si_{30}Ga_{16}$ clathrates in terms of hybridization can be perceived from their different valence electron density distributions. This is demonstrated in Fig. 8, where the electronic charge distributions in real space are shown as contour maps of the valence electron densities for $Ba_8Si_{40}Ga_6$ and $Ba_8Si_{30}Ga_{16}$, plotted on the (100) plane through Ba (2*a*) sites and the six- membered rings of Si(Ga) (see Fig. 1). The two Ba sites of each figure correspond to those at the centers of the Si_{20} cages.

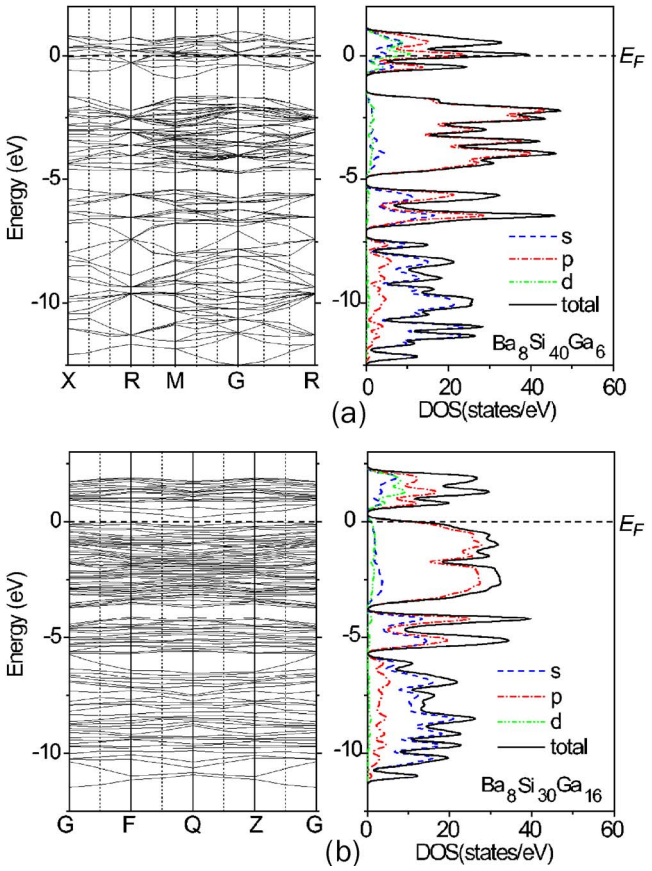

FIG. 7. (Color online) Band structures and density of states for (a) $Ba_8Si_{40}Ga_6$ and (b) $Ba_8Si_{30}Ga_{16}$. Density of states is calculated using 0.1 eV Gaussian broadening of the band structure. The Fermi levels are denoted by broken horizontal lines.

As shown in Fig. 8, Ga substitution significantly reduces the integrity of the charge distribution spread uniformly across the Si cagelike network. Such changes to the sp^3 network may further suppress the superconductivity of the Ga16 material.[20] Comparing $Ba_8Si_{40}Ga_6$ as shown in Fig. 8(a) with Ga-free Ba_8Si_{46},[20] no distinct differences are observed in valence electron densities on the Ba and Si sites, and the presence of Ga at the 6*c* sites leads to reduced charge transfer, less charge density localized around the Ga sites, and fewer *p* electrons on the Ga atoms. There is an enhanced electron density between the 6*c* site and its Si neighbors, resulting in a local maximum of the charge density [seen in Fig. 8(a)]. This shows that Ga orbitals hybridize strongly with the host Si cage orbitals. In the case of heavy Ga substitution, besides filled 6*c* sites, 6*i* and 24*k* sites are partially occupied by Ga in $Ba_8Si_{30}Ga_{16}$. In this case there is a significantly larger charge density along the Si-Ga bond direction, showing that Ga orbitals hybridize more strongly in this case.

To show the effect of Ga substitution on the charge distributions at the Fermi level, corresponding to states which play a crucial role in superconductivity, contour maps of the electron densities at the Fermi level are shown in Fig. 9. For $Ba_8Si_{40}Ga_6$, the electrons are distributed relatively uniformly on the Si framework sites and Ba sites. In contrast, the electron distribution spreads out much less effectively for the band-edge states corresponding to the Fermi level in $Ba_8Si_{30}Ga_{16}$, and the states appear to be poorly connected, reminiscent of the impurity band model for the conductivity that has been proposed for other type-I clathrates.[38]

IV. DISCUSSION

Isotope effect measurements have revealed that superconductivity in Ba_8Si_{46} is of the classic type, arising from the

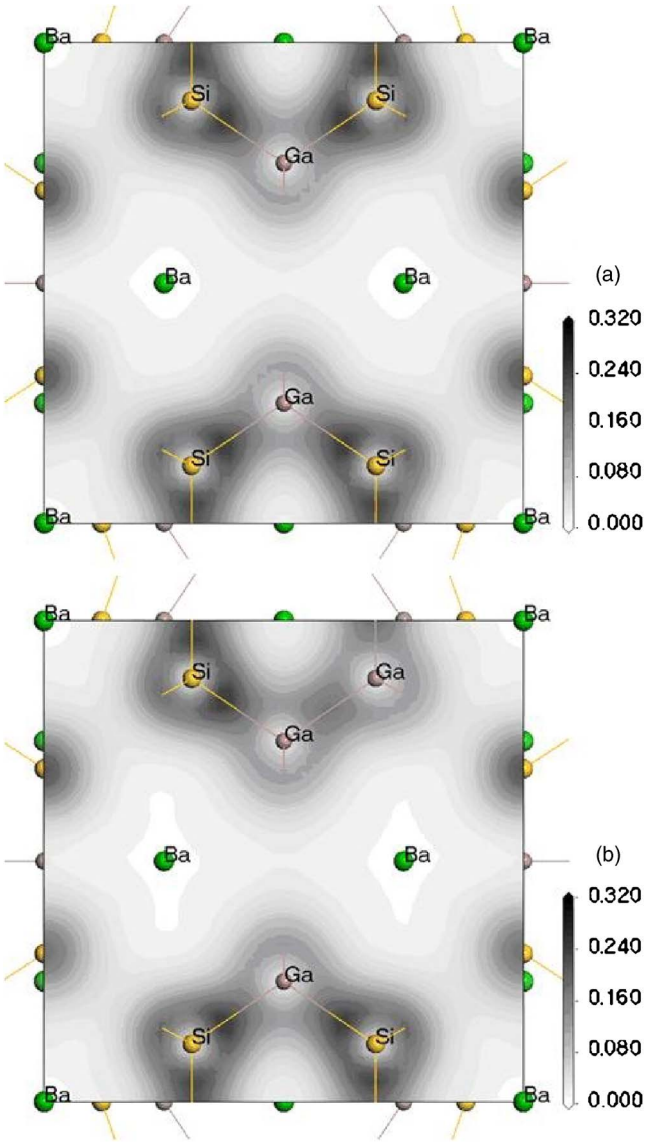

FIG. 8. (Color online) Contour maps of the valence electron densities of (a) $Ba_8Si_{40}Ga_6$ and (b) $Ba_8Si_{30}Ga_{16}$ on the (100) plane.

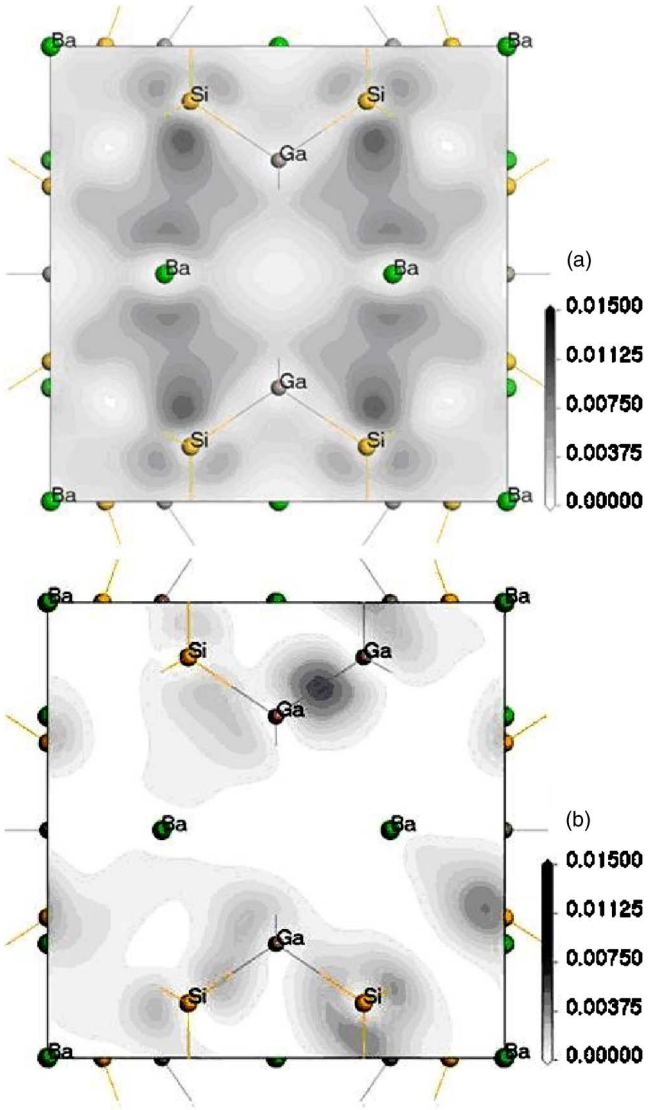

FIG. 9. (Color online) Contour maps of the electron densities at the Fermi level of $Ba_8Si_{40}Ga_6$ (upper) and $Ba_8Si_{30}Ga_{16}$ (lower) on the (100) plane.

electron-phonon interaction.[17] In the conventional BCS theory for phonon-mediated superconductivity,[39] T_C can be estimated in terms of the Debye temperature Θ_D, the effective electron-phonon repulsive interaction μ^*, and the electron-phonon coupling constant λ_{ep}:

$$T_C = \frac{\Theta_D}{1.45} \exp\left(\frac{-1.04(1+\lambda_{ep})}{\lambda_{ep} - \mu * (1+0.62\lambda_{ep})}\right).$$

Furthermore, λ_{ep} can be expressed as the product of $N(E_F)$ and the average electron pairing interaction V_{ep}.

The Debye temperature $\Theta_D = 370$ K has been evaluated by specific heat measurement in Ba_8Si_{46}.[17] We make the reasonable assumption that Θ_D should have the same magnitude in $Ba_8Si_{40}Ga_6$. The estimation of λ_{ep} from T_C using the McMillan formula is not very sensitive to the value of Θ_D. Moreover, we set the effective electron-phonon repulsion μ^* to 0.24, which was estimated for Ba_8Si_{46}.[17,21] From this we find that $\lambda_{ep} = 0.78$, somewhat smaller than the value found for Ba_8Si_{46} ($\lambda_{ep} = 1.05$). This implies that Ga-doped $Ba_8Si_{40}Ga_6$ has a relative weaker electron-phonon coupling. Using $N(E_F) = 38$ states/eV for $Ba_8Si_{40}Ga_6$, the average electron pairing interaction V_{ep} is estimated as 20.5 meV. This value is also smaller than that obtained for Ga-free Ba_8Si_{46}, 24 meV. It thus appears that the T_C decrease with Ga doping can be partially assigned to the weakening of electron-phonon coupling as well as a decrease of the density of states at the Fermi level; however, given the range of T_C observed in various samples of Ba_8Si_{46}, it remains possible that the observed reduction in $Ba_8Si_{40}Ga_6$ is due entirely to the small drop in $N(E_F)$.

In conclusion, we have presented a combined experimental and theoretical study of the effect of Ga substitution on the superconductivity of the type-I clathrate $Ba_8Si_{46-x}Ga_x$. In Ga-doped clathrates, the Ga state is found to be strongly hybridized with the cage conduction band state. Ga substitu-

tion results in a shift toward a lower energy, a decrease of $N(E_F)$, a lowering of the carrier concentration, and a breakage of the integrity of the sp^3-hybridized networks. These play key roles in the suppression of superconductivity. For $Ba_8Si_{40}Ga_6$, the onset of the superconducting transition occurs at $T_C \approx 3.3$ K. The investigation of the magnetic superconducting state shows that $Ba_8Si_{40}Ga_6$ is a type-II superconductor. The critical magnetic fields H_{C1} and H_{C2} were measured to be $H_{C1} \approx 35$ Oe and $H_{C2} \approx 8.5$ kOe. We deduce the London penetration depth $\lambda \approx 3700$ Å and the coherence length $\xi \approx 200$ Å. Our estimate of the electron-phonon coupling reveals that $Ba_8Si_{40}Ga_6$ is a moderate phonon-mediated BCS superconductor.

ACKNOWLEDGMENTS

This work was supported in part by the National Natural Science Foundation of China (Grant No. 50372005), the Robert A. Welch Foundation (Grant No. A-1526), the UPRM-CID seed program (Grant No. SM-07-14), and the National Science Foundation PREM program (Grant No. 0351449).

*Corresponding author. Electronic address: ylibp@hotmail.com
†Corresponding author. Electronic address: jhross@tamu.edu

[1] J. L. Cohn, G. S. Nolas, V. Fessatidis, T. H. Metcalf, and G. A. Slack, Phys. Rev. Lett. **82**, 779 (1999).
[2] G. S. Nolas, T. J. R. Weakley, J. L. Cohn, and R. Sharma, Phys. Rev. B **61**, 3845 (2000).
[3] S. Bobev and S. Sevov, J. Solid State Chem. **153**, 92 (2000).
[4] H. Shimizu, T. Kume, T. Kuroda, S. Sasaki, H. Fukuoka, and S. Yamanaka, Phys. Rev. B **68**, 212102 (2003).
[5] S. B. Roy, K. E. Sim, and A. D. Caplin, Philos. Mag. A **65**, 1445 (1992).
[6] J. S. Tse, K. Uehara, R. Rousseau, A. Ker, C. I. Ratcliffe, M. A. White, and G. MacKay, Phys. Rev. Lett. **85**, 114 (2000).
[7] B. B. Iversen, A. E. C. Palmqvist, D. E. Cox, G. S. Nolas, G. D. Stucky, N. P. Blake, and H. Metiu, J. Solid State Chem. **149**, 455 (2000).
[8] Weiping Gou, Yang Li, Ji Chi, Joseph H. Ross, Jr., M. Beekman, and G. S. Nolas, Phys. Rev. B **71**, 174307 (2005).
[9] R. P. Hermann, V. Keppens, P. Bonville, G. S. Nolas, F. Grandjean, G. J. Long, H. M. Christen, B. C. Chakoumakos, B. C. Sales, and D. Mandrus, Phys. Rev. Lett. **97**, 017401 (2006).
[10] B. C. Sales, B. C. Chakoumakos, R. Jin, J. R. Thompson, and D. Mandrus, Phys. Rev. B **63**, 245113 (2001).
[11] T. Kawaguchi, K. Tanigaki, and M. Yasukawa, Appl. Phys. Lett. **77**, 3438 (2000).
[12] Yang Li and J. H. Ross, Jr., Appl. Phys. Lett. **83**, 2868 (2003).
[13] Y. Li, J. Chi, W. P. Gou, S. Khandekar, and J. H. Ross, Jr., J. Phys.: Condens. Matter **15**, 5535 (2003).
[14] Y. Li, W. P. Gou, J. Chi, V. Goruganti, and J. H. Ross, Jr., in *27th International Conference on the Physics of Semiconductors*, edited by J. Menéndez and C. G. Van der Walle, AIP Conf. Proc. No. 772 (AIP, Melville, NY, 2005), p. 331.
[15] H. Kawaji, H. O. Horie, S. Yamanaka, and M. Ishikawa, Phys. Rev. Lett. **74**, 1427 (1995).
[16] S. Yamanaka, E. Enishi, H. Fukuoka, and M. Yasukawa, Inorg. Chem. **39**, 56 (2000).
[17] K. Tanigaki, T. Shimizu, K. M. Itoh, J. Teraoka, Y. Moritomo, and S. Yamanaka, Nat. Mater. **2**, 653 (2003).
[18] S. Saito and A. Oshiyama, Phys. Rev. B **51**, 2628 (1995).
[19] K. Moriguchi, M. Yonemura, A. Shintani, and S. Yamanaka, Phys. Rev. B **61**, 9859 (2000).
[20] Yang Li, Y. Liu, N. Chen, G. H. Cao, Z. S. Feng, and J. H. Ross, Jr., Phys. Lett. A **345**, 398 (2005).
[21] D. Connétable, V. Timoshevskii, B. Masenelli, J. Beille, J. Marcus, B. Barbara, A. M. Saitta, G.-M. Rignanese, P. Mélinon, S. Yamanaka, and X. Blase, Phys. Rev. Lett. **91**, 247001 (2003).
[22] V. L. Kuznetsov, L. A. Kuznetsova, A. E. Kaliazin, and D. M. Rowe, J. Appl. Phys. **87**, 7871 (2000).
[23] A. C. Larson and R. B. von Dreele, Los Alamos National Laboratory Report No. LAUR 86-748, 2000 (unpublished).
[24] B. H. Toby, J. Appl. Crystallogr. **34**, 210 (2001).
[25] Y. G. Zhang, P. L. Lee, G. S. Nolas, and A. P. Wilkinson, Appl. Phys. Lett. **80**, 2931 (2002).
[26] A. Bentien, B. B. Iversen, J. D. Bryan, G. D. Stucky, A. E. C. Palmqvist, A. J. Schultz, and R. W. Henning, J. Appl. Phys. **91**, 5694 (2002).
[27] B. Eisenmann, H. Schafer, and R. Zagler, J. Less-Common Met. **118**, 43 (1986).
[28] J. I. Goldstein, D. B. Williams, and G. Cliff, in *Principles of Analytical Electron Microscopy*, edited by D. C. Joy, A. D. Romig, Jr., and J. I. Goldstein (Plenum Press, New York, 1986), pp. 155–217.
[29] J. Bardeen, L. N. Cooper, and J. R. Schrieffer, Phys. Rev. **108**, 1175 (1957).
[30] V. L. Ginzburg and L. D. Landau, Zh. Eksp. Teor. Fiz. **20**, 1064 (1950).
[31] C.-R. Hu, Phys. Rev. B **6**, 1756 (1972).
[32] I. M. Gat, Y. Fudamoto, and A. Kinkhabwala, Physica B **289**, 385 (2000).
[33] R. Viennois, P. Toulemonde, C. Paulsen, and A. San-Miguel, J. Phys.: Condens. Matter **17**, L311 (2005).
[34] M. C. Payne, M. P. Teter, D. C. Allan, T. A. Arias, and J. D. Joannopoulos, Rev. Mod. Phys. **64**, 1045 (1992).
[35] K. Moriguchi, M. Yonemura, A. Shintani, and S. Yamanaka, Phys. Rev. B **61**, 9859 (2000).
[36] N. P. Blake, S. Latturner, J. D. Bryan, G. D. Stucky, and H. Metiu, J. Chem. Phys. **115**, 8060 (2001).
[37] P. Toulemonde, A. San Miguel, A. Merlen, R. Viennois, S. Le Floch, C. Adessi, X. Blase, and J. L. Tholence, J. Phys. Chem. Solids **67**, 1117 (2006).
[38] G. S. Nolas, J. L. Cohn, J. S. Dyck, C. Uher, and J. Yang, Phys. Rev. B **65**, 165201 (2002).
[39] W. L. McMillan, Phys. Rev. **167**, 331 (1968).